Closed-Loop Control of Magnetic Modular Cubes for 2D Self-Assembly

Yitong Lu[1†], Anuruddha Bhattacharjee[2†], Conlan C. Taylor[1], Julien Leclerc[1], Jason M. O'Kane[3], MinJun Kim[2*], and Aaron T. Becker[1*]

***Abstract*—Reconfigurable modular robots can dynamically assemble/disassemble to accomplish the desired task better. Magnetic modular cubes are scalable modular subunits with embedded permanent magnets in a 3D-printed cubic body and can be wirelessly controlled by an external, uniform, time-varying magnetic field. This paper considers the problem of self-assembling these modules into desired 2D polyomino shapes using such magnetic fields. Although the applied magnetic field is the same for each magnetic modular cube, we use collisions with workspace boundaries to rearrange the cubes. We present a closed-loop control method for self-assembling the magnetic modular cubes into polyomino shapes, using computer vision-based feedback with re-planning. Experimental results demonstrate that the proposed closed-loop control improves the success rate of forming 2D user-specified polyominoes compared to an open-loop baseline. We also demonstrate the validity of the approach over changes in length scales, testing with both $10\,\mathrm{mm}$ edge length cubes and $2.8\,\mathrm{mm}$ edge length cubes.**

I. Introduction

Reconfigurable modular robots (RMRs) at mesoscale (milli- and microscales) have seen substantial development in recent years due to an increasing interest in modular designs, which are capable of reconfiguration for adapting to uncertain environments [1]–[3]. Reconfigurability improves a system's reusability and range of application while reducing the dependence on human input [4], [5]. Robot designs and algorithms have been developed to complete more complex tasks, such as part manipulation, assembly sequencing, and motion planning, using mechanically actuated and coupled units [6]–[8]. RMRs using magnetic materials have also been of interest to researchers, particularly the use of magnetic fields for actuation [9] and magnetic coupling to secure modules in rigid formations while still allowing easy disconnection for reassembly into different structures [10]. Numerous designs for magnetic RMRs have been proposed and tested by researchers, including millimeter-scale cube modules with electrostatic anchoring capabilities [11], magnetic quadrupoles with dipole tuning [12], programmable cuboids [13], various bio-inspired soft robots [14], and shape-morphing soft materials [15].

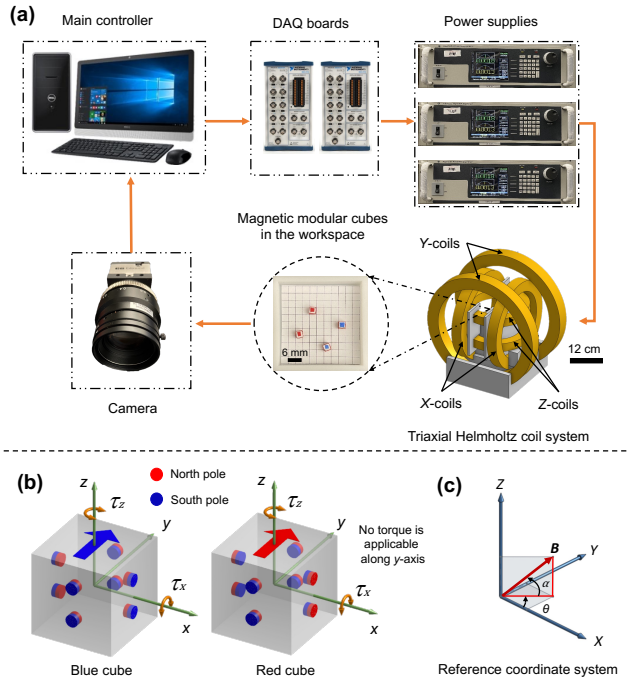

Fig. 1. **(a)** Experimental setup. **(b)** Design variations of magnetic modular cubes (blue and red cubes) with embedded cylindrical permanent magnets in faces. **(c)** Reference coordinate system for the external magnetic field.

The magnetic modular cubes (MMCs) shown in Fig. 1 can be controlled by a global magnetic field, with applications in mesoscale manufacturing, manipulation, and construction in *ex vivo* and *in vitro*. In these applications, vision systems (e.g., camera, X-ray, and CT) provide feedback to improve performance. Due to the MMCs' cubic design, magnetically connected structures of MMCs are polyominoes in 2D and polycubes in 3D [16]. In our previous work [17], we provided a family of designs for MMCs and counted how many configurations were possible for each design as a function of the number of modules. In addition, we developed a motion planner based on a low-fidelity simulator for 2D self-assembly and applied the motion planner in open-loop [18]. Low-fidelity simulations simplify the physics and configuration space to speed up the simulation. For example, we used unit-length squares to represent cubes in 2D and assumed that all modules in the simulation move at the same speed in the same direction unless they encounter workspace boundaries. We also assumed that cubes only assemble if they are in adjacent cells in the

Manuscript received: February 24, 2023; Revised: May 18, 2023; Accepted: June 27, 2023.

This paper was recommended for publication by Editor M. Ani Hsieh upon evaluation of the Associate Editor and Reviewers' comments.

This work was supported by the NSF under Grant Nos. [IIS-1553063, IIS-1849303, IIS-2130775, CNS-1932572].

[1]Authors are with the University of Houston, Houston, TX 77204 USA {ylu36, ctaylor16, jleclerc, atbecker}@uh.edu.

[2]Authors are with Southern Methodist University, Dallas, TX 75275 USA abhattacharjee@smu.edu, mjkim@lyle.smu.edu.

[3]Author is with the Texas A&M University, College Station, TX 77843 USA jokane@tamu.edu.

[†]Equally contributed to the paper. [*]Co-corresponding authors.

Digital Object Identifier (DOI): see top of this page.

workspace and their magnets have opposite polarity. High-fidelity simulations utilize more realistic physics to represent the task. A high-fidelity simulation of the MMCs would consider the materials of the cubes and the workspace, the design of the cubes, forces applied to and between cubes, motion modes, and so on.

For motion planning, choosing the fidelity of the simulation introduces a trade-off between computational efficiency and robustness [19], [20]. Planning with a high-fidelity model is likely to result in a more robust plan by reducing environmental uncertainty, but it is time-consuming. When navigating in a simple environment, it can be unnecessary. The robotics platform in this paper uses a simple workspace (no obstacles except the boundary). The goal is to quickly generate a motion path to complete a 2D self-assembly task. However, simple models that quickly generate plans may fail to capture unexpected changes like path deviation and pre-assembly, which may lead to task failures.

Therefore, this paper presents a closed-loop control method that uses a low-fidelity motion planner with a re-planning technique to improve the success rate of self-assembling 2D user-specified target polyominoes. Our motion planner uses color differences to differentiate the two variations of cubes. Alternate methods could be used for different applications. **The contributions of this paper are: 1) An upgraded controller that uses equations with coil design parameters to generate magnetic fields with any magnitude and frequency, 2) an improved motion planner accounting for rotations to expand the set of reachable polyominoes, 3) a vision-based cube tracking system for feedback, and 4) a closed-loop control method for self-assembly of user-specified polyominoes of MMCs.**

II. Experimental Setup

A. Hardware description

The electromagnetic manipulator used in this study is a nested triaxial Helmholtz coil system (Fig. 1(a)), which has three pairs of electromagnetic coils. Each coil pair is connected to a power supply (Kepco, BOP 50-20 MG) controlled by a National Instruments data acquisition (DAQ) board. A customized Python program was developed and used to send signal outputs to the interfaced DAQ boards to generate a uniform magnetic field over the workspace with time-dependent magnitude and frequency. The DAQ boards then direct the signals to the connected power supplies. Experiments were conducted inside the nested Helmholtz coil system on a 3D-printed flat workspace with a boundary wall (Fig. 1(a)). We used two different-sized workspaces (each having 11×11 unit cells) for experiments. A larger workspace with a clear area of $110 \times 110\,\mathrm{mm}^2$ was used for cubes with $10\,\mathrm{mm}$ edges, while a smaller workspace with an area of $33 \times 33\,\mathrm{mm}^2$ was used for cubes with $2.8\,\mathrm{mm}$ edges. The workspace was located at the center of the coil system, and all experiments were performed on the X–Y plane (where we assumed $Z = 0\,\mathrm{mm}$). A digital camera (color CCD) was located at the top of the workspace for tracking the cubes. The tracking process is described in detail in Section II-D. The controller and the tracker regulate the magnetic field's strength. The motion tracker measures the size of the largest structure in the workspace, and the motion controller provides a sufficient magnetic field to actuate structures of this size.

B. Design and fabrication of the magnetic modular cubes

Two sizes of modular cubes with $10\,\mathrm{mm}$ and with $2.8\,\mathrm{mm}$ edge lengths were used in this study. Design specifications of the modular cubes and the embedded magnets are described in detail in our previous work [18]. To help detect individual cubes in an assembled structure, we added red and blue colored electrical tape (with a thickness of $0.2\,\mathrm{mm}$) to the top face of the cubes. Furthermore, we added white-colored electrical tape (with a thickness of $0.2\,\mathrm{mm}$) to the side faces of the cubes with $2.8\,\mathrm{mm}$ edges to facilitate disassembly.

C. Magnetic control method and motion modes

The Helmholtz coil system can create a uniform magnetic field with an arbitrary orientation at the center of the coil system. Figure 1(c) shows the reference coordinate system for the external magnetic field. The applied magnetic flux density $\boldsymbol{B}$ can be calculated with

$$\boldsymbol{B} = \begin{bmatrix} B_X \\ B_Y \\ B_Z \end{bmatrix} = B \begin{bmatrix} \cos(\theta)\cos(\alpha) \\ \sin(\theta)\cos(\alpha) \\ \sin(\alpha) \end{bmatrix}, \tag{1}$$

$$\text{and} \quad \boldsymbol{B} = \frac{8\mu_0}{5\sqrt{5}} \left[\frac{V_X N_X}{r_X R_X}, \frac{V_Y N_Y}{r_Y R_Y}, \frac{V_Z N_Z}{r_Z R_Z} \right]^\top, \tag{2}$$

where B_X, B_Y, and B_Z are the components along X, Y and Z-axes; B is the magnitude; R_X, R_Y, and R_Z are the coil resistances; r_X, r_Y, and r_Z are the coil radii; N_X, N_Y, and N_Z are the number of turns for each coil; μ_0 is the permeability of free space, α is the pitch angle (in the vertical plane), and θ is the yaw angle (in the X-Y plane). The applied voltages (V_X, V_Y, and V_Z) to each coil pair are calculated by solving (1) and (2). The general equation for a coil voltage is $V(t) = RI(t) + L\frac{dI(t)}{dt}$, where I, R, and L are the coil current, resistance, and inductance. We assume that $L\frac{dI(t)}{dt}$ is much smaller than $RI(t)$ and exclude it from (2). The constants in (2) are derived from the Biot-Savart law (Eq. 7 in [21]).

A force-free magnetic torque ($\boldsymbol{\tau} = [\tau_x, 0, \tau_z]^\top$) is induced to the modular cube under a uniform magnetic field with the flux density $\boldsymbol{B}$, aligning the cube's net magnetic moment ($\boldsymbol{M}_{net}$) with the direction of the applied field. We can compute the applied torque

$$\boldsymbol{\tau} = \boldsymbol{M}_{net} \times \boldsymbol{B}. \tag{3}$$

The magnetic torques on the modular cubes enable pivot walking. Pivot walking actuates individual cubes (or cube assemblies) in a direction that is perpendicular to their $\boldsymbol{M}_{net}$. At the beginning of experiments, $\boldsymbol{M}_{net}$ of the individual magnetic cubes are aligned to the Y-axis (with $\theta = \pi/2$). Then, a magnetic torque about the Z-axis can be applied to rotate the $\boldsymbol{M}_{net}$ of the cubes toward any direction of choice. The yaw angle before and after the rotation can be referred to as θ_0 and θ_G. A rapid change (within 0.8 seconds) of the yaw direction θ, with a change of the angle $|\theta_G - \theta_0| \geq 140^\circ$ (by

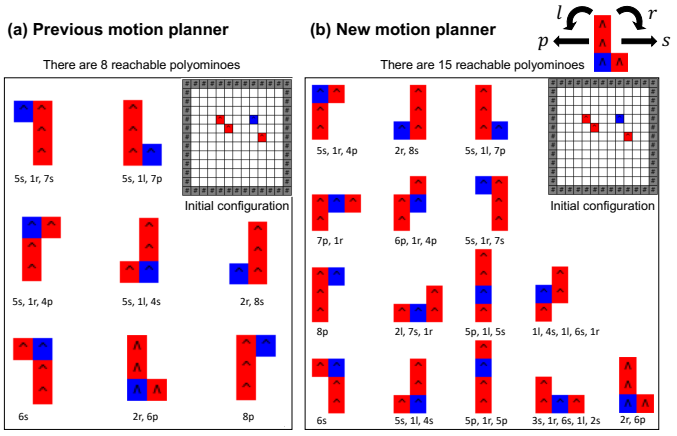

Fig. 2. Comparison of the self-assembly results between **(a)** the previous motion planner [18] and **(b)** the new motion planner. Arrows on squares indicate direction of the net magnetization (from magnetic south to north pole). Underneath each polyomino is listed the shortest construction sequence.

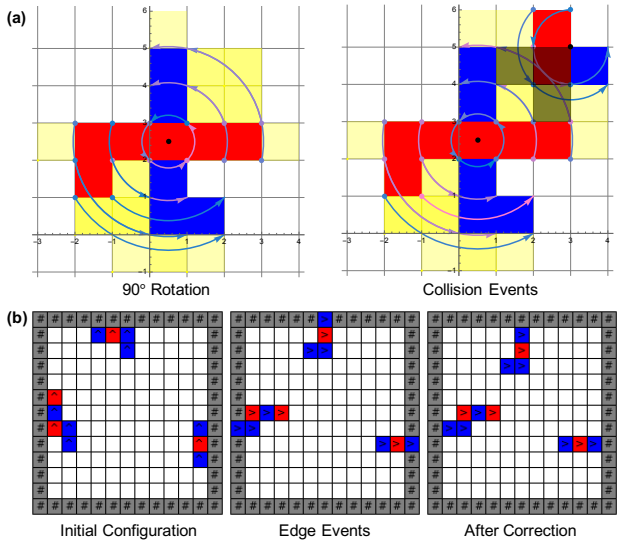

Fig. 3. **(a)** Illustrations show the result of the rotation checker when applying a 90° rotation and detecting collision events for one polyomino (left) and two (right). Black points indicate the rotation centers. The red polyomino represents the initial configuration, and the blue polyomino represents the end position. Yellow cells indicate cells intersected during rotation. Gray cells indicate intersected cells that overlap. **(b)** Illustrations show the result of the rotation checker correcting edge events.

either counter-clockwise (CCW) or clockwise (CW) applied rotational magnetic torques τ_z and $-\tau_z$, respectively), can create disassembly of an assembled structure [18]. To avoid any undesired disassembly, we implemented a controller that smoothly changes the applied magnetic field from the initial angle θ_0 to the goal angle θ_G. The angular coordinates for an acceleration control that changes the orientation from θ_0 to θ_G as quickly as possible using a maximum acceleration $a_{\max}$ are computed as follows[1]:

$$\begin{aligned} \theta_\Delta &= \operatorname{atan2}(\sin(\theta_G-\theta_0),\cos(\theta_G-\theta_0)),\\ t_h &= \sqrt{|\theta_\Delta/a_{\max}|}, \quad s_{\theta_\Delta}=\operatorname{sign}(\theta_\Delta), \quad t_i = i\cdot t_\Delta, \qquad (4)\\ \theta_i &= \theta_0 + s_{\theta_\Delta}\frac{a_{\max}}{2}\begin{cases} t_i^2 & t_i \le t_h \\ 4t_h t_i - 2t_i^2 - 2t_h^2 & \text{otherwise}\end{cases}. \end{aligned}$$

[1]code & derivation at mathworks.com/matlabcentral/fileexchange/128539

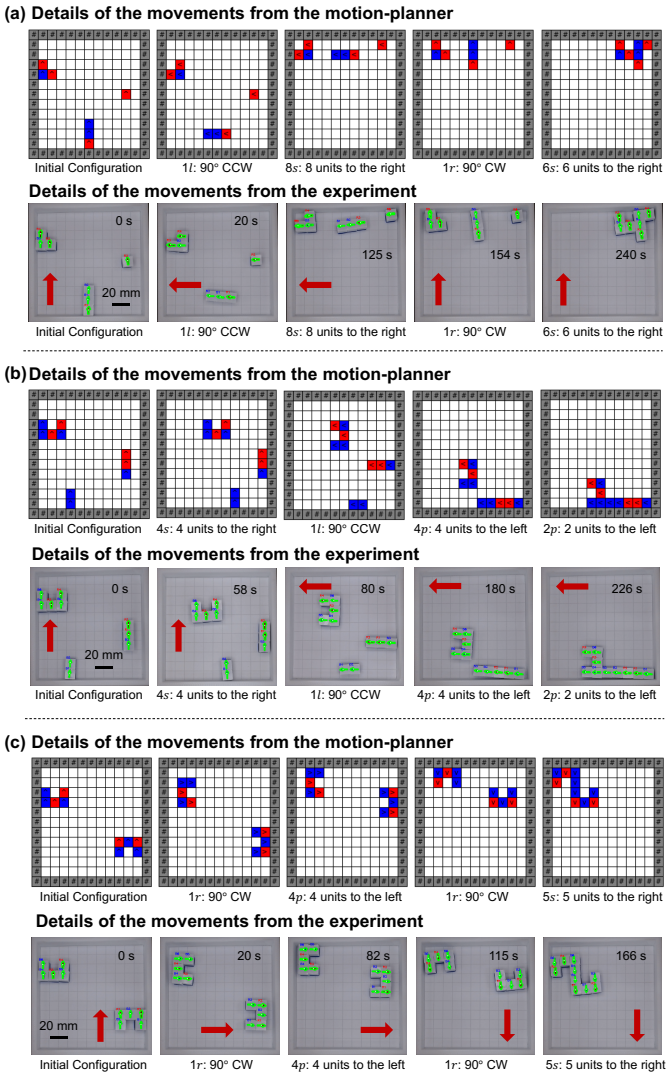

Fig. 4. Closed-loop controlled self-assembly to form target polyominoes using cubes with 10 mm edge lengths. The red arrows indicate the direction of the applied magnetic field. See supplementary video 1 for these demonstrations.

This produces a vector of angular positions every t_Δ seconds. In our experiments, using $a_{\max} = 4\pi$ rad s^{-2} rotated polyominoes smoothly without disassembly at both length scales.

D. Motion tracker

The motion tracking program identifies the color and position of the MMCs using the Python OpenCV library. The MMCs are thresholded in HSV color space and de-noised. Then a contour is constructed for each MMC, and the centroid of each MMC is calculated. Their orientation on the X-Y plane can be retrieved from the yaw angle θ of the applied external magnetic field from (1).

We manually cropped the image based on the workspace boundary for each experiment, so the image resolution is not constant (around 312×312 pixel^2). We captured images of the cubes before and after each external magnetic input motion step. The image information from the tracker is also used to convert the MMCs' positions between the hardware [pixels] and simulation [workspace coordinates] configurations, as described in Section IV by performing a linear transformation.

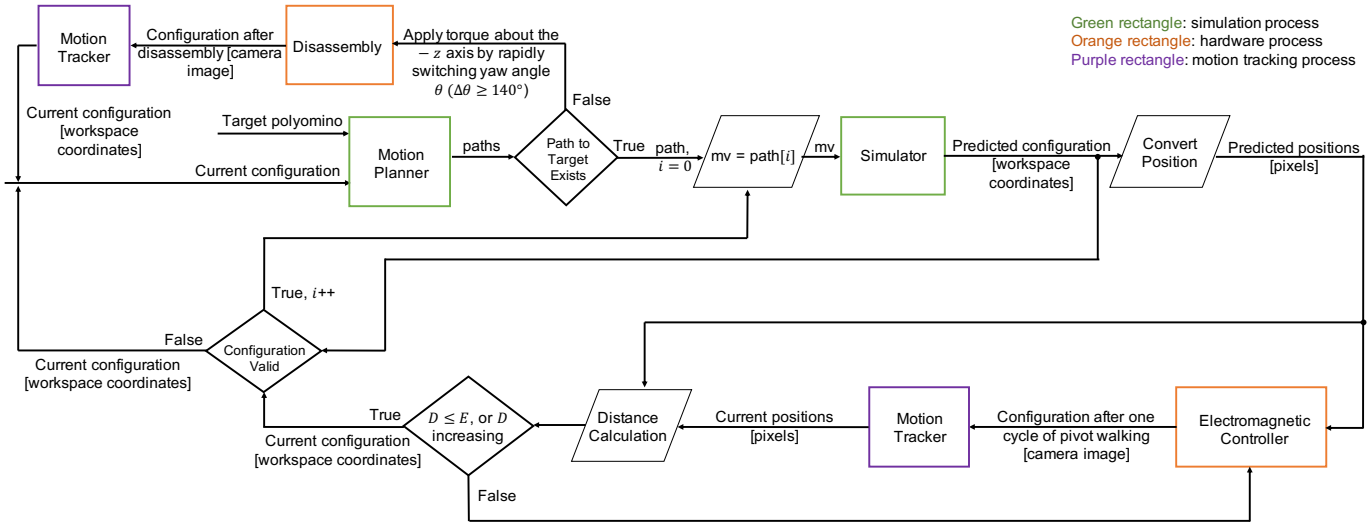

Fig. 5. Block diagram presenting a closed-loop control method of the magnetic modular cubes using vision-based feedback. *Path to target exists* checks whether a path exists to generate the target polyomino from the current configuration. *Configuration valid* checks whether a pre-assembly occurs, a hardware configuration different from the planned configuration. If no pre-assembly occurred, the configuration is valid.

III. Motion Planner

In our previous works [17], [18], we devised a low-fidelity simulator based on the hardware experiment environment. We implemented a self-assembly algorithm, which takes the initial configuration of modular cubes as input and returns all reachable polyominoes and the shortest construction sequence to form each reachable polyomino. Figure 2(a) shows an example of the self-assembly result using the previous motion planner. Eight reachable polyominoes can be constructed from the initial configuration as shown in the top right corner of Fig. 2(a), and only L-shapes are reachable. The shortest step sequence to construct each polyomino is listed beneath it. All translation steps are based on the net magnetization direction. At each step, cubes can move one unit length to the left (p for port) or right (s for starboard), or rotate in-place clockwise (r to the right) a quarter-turn or counterclockwise (l to the left) a quarter-turn.

However, our previous simulator did not consider rotations to polyomino structures in certain cases, which we refer to as *edge events* and *collision events*. *Edge events* occur when rotating an assembled structure results in the structure overlapping with a workspace boundary. *Collision events* are characterized by a collision between assembled structures during rotation. The previous motion planner also did not apply rotation steps when cubes formed sub-assemblies. In this paper, we improved the motion planner by adding a rotation checker to establish a set of rules for resolving these events and enabling rotations with both individual modules and sub-assemblies. The new planner can find more reachable polyominoes from the same initial configuration than the previous planner (Fig. 2(b)). For example, Z-shapes and I-shapes can now be generated.

The function implemented in the rotation checker takes polyominoes, rotation points, and a rotation angle as inputs and then computes the cells that cubes sweep over during a rotation. Figure 3(a) shows the result of the rotation checker when applying $90°$ rotation to an L-shape polyomino and detecting collision events for two polyominoes rotate at different rotation points (black points). Our magnetic modular cubes perform in-place rotation. In the motion planner, we define the rotation point at the polyomino's center of mass, rounded to the center of the nearest grid cell. The function iterates over each vertex in every cube in a polyomino in the workspace, then finds the grid cells over which the $90°$ arc passing between the cube's original and final positions sweeps. All grid cells covered by the arcs are collected in a list. When there are multiple polyominoes in the workspace, these lists are compared. If any overlap occurs, we terminate the search along the path that produces the collision event. Figure 3(b) shows the result of correcting the edge events. Edge events are resolved by shifting the polyomino until all cubes in the polyomino are in the workspace.

IV. Closed-Loop Control of the MMCs

Our previous work [18] implemented the motion planner using open-loop control. Open-loop control requires a calibration procedure. We collected data that measured a modular cube's mean X and Y displacement and calculated the required number of pivot walking cycles for each cube size to move a given unit step. However, the distance traveled by a polyomino in one cycle of pivot walking depends on the length between the polyomino's north and south pivot points, which may vary during different experiments if the MMCs assemble or disassemble. Therefore, we implemented a closed-loop control method to move MMCs and their assemblies without requiring a calibration procedure (Fig. 5). The method combines the motion tracker and motion planner with the external electromagnetic controller to move the MMCs using vision-based feedback. First, the motion planner calculates a path to form the target polyomino. Then, the simulation applies the first movement step `mv` from the path and predicts the position of each MMC. Next, we convert the predicted positions in the simulation [workspace coordinates] to hardware [pixels] as

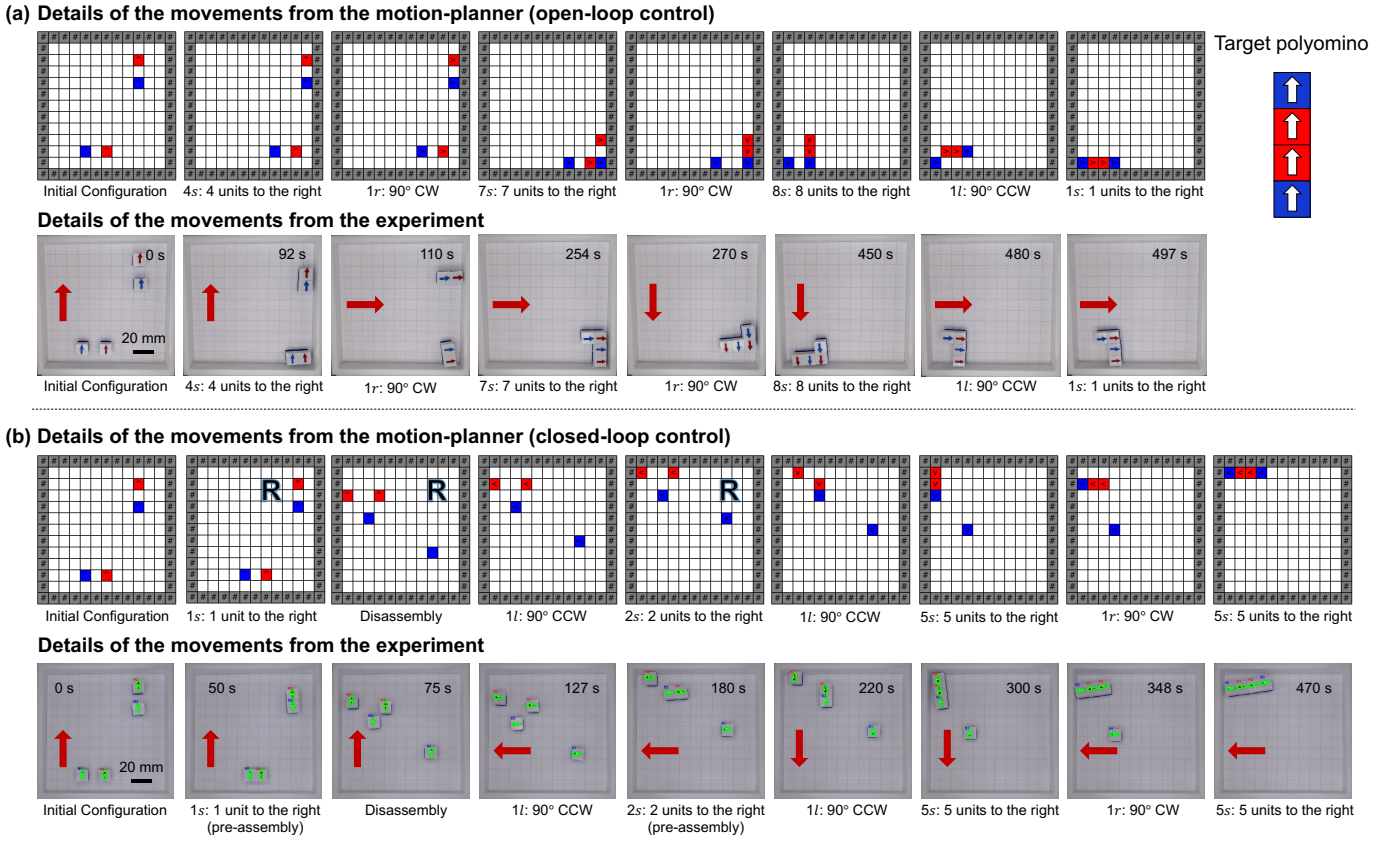

Fig. 6. Comparison of the open-loop and closed-loop controlled self-assembly to form the target I-shape polyomino using cubes with 10 mm edges. **(a)** Details of movements from the motion planner and video snapshots showing a failure during open-loop implementation. **(b)** Details of movements from the motion planner and snapshots from the motion tracker showing closed-loop implementation. **R** indicates the motion planner re-plans the path to follow based on the current configuration from the hardware. Red arrows point in the direction of the applied magnetic field.

goal positions G_j, where j indicates the j-th cube. The electromagnetic controller generates pivot walking commands to move the hardware MMCs to the goal positions. We calculate the average distance D along the translation vector v between the MMCs' current positions C_j and their goal positions G_j. That is, $D = \Sigma_{j=1}^{n}(|G_{j,v} - C_{j,v}|)/n$, where n is the number of MMCs in the workspace. The electromagnetic controller moves the cubes until $D \leq E$, where E is a predetermined error threshold. We also exit the loop if the current distance exceeds the previous distance. In the experiments conducted in Section V, we used E of 12 pixels to control cubes with 10 mm edge lengths and 8 pixels for cubes with 2.8 mm edge lengths. These values correspond to half of the respective edge length in the corresponding resolution.

Another challenge with open-loop control is that MMCs can change configuration during manipulation. Magnetic dipole particles tend to form chain-like structures. Due to dipole symmetry, these are low-energy configurations [12]. During pivot walking, the MMCs may reconfigure into undesired lower-energy configurations. We call this pre-assembly. Therefore, we implemented a re-planning technique to the closed-loop control algorithm (Fig. 5) that takes the target polyomino and current configuration as input. The motion planner first determines if the target polyomino is reachable from the configuration. If no path exists, it disassembles the cubes to generate a new configuration. If a path to the target exists, the system starts moving the MMCs, making them follow the path using vision-based feedback. After following each movement step mv, the system checks whether the obtained configuration is *valid*. A *valid* hardware configuration matches the configuration predicted by the simulator. An undesired assembly or disassembly will cause the configuration to be invalid. The system applies the next movement step from the path if the configuration is valid. If the configuration is not valid, we restart our motion planner.

A target polyomino is a set of connected colored cubes with specified coloring and orientations. Our previous work [17] counts the number of possible configurations as a function of the number of modules and enumerates all arrangements for up to 20 modules in 2D. For example, the number of fixed polyominoes is 19, with 4 cubes without coloring, and the maximum number of colored polyominoes is 64, with 2 blue cubes and 2 red cubes. Therefore, forming a specified colored polyomino is challenging. Since all of our cubes have the same shape, for many applications, the specific coloring is not necessary. To further improve the success rate of self-assembly, we propose an alternate method that only considers the shape, not the coloring of the cubes. To find the best suitable path to form the target shape, we save the paths to form polyominoes with the same shape in a list, then sort the list by finding the shortest sequence to the first subassembly, which reduces the probability of pre-assembly.

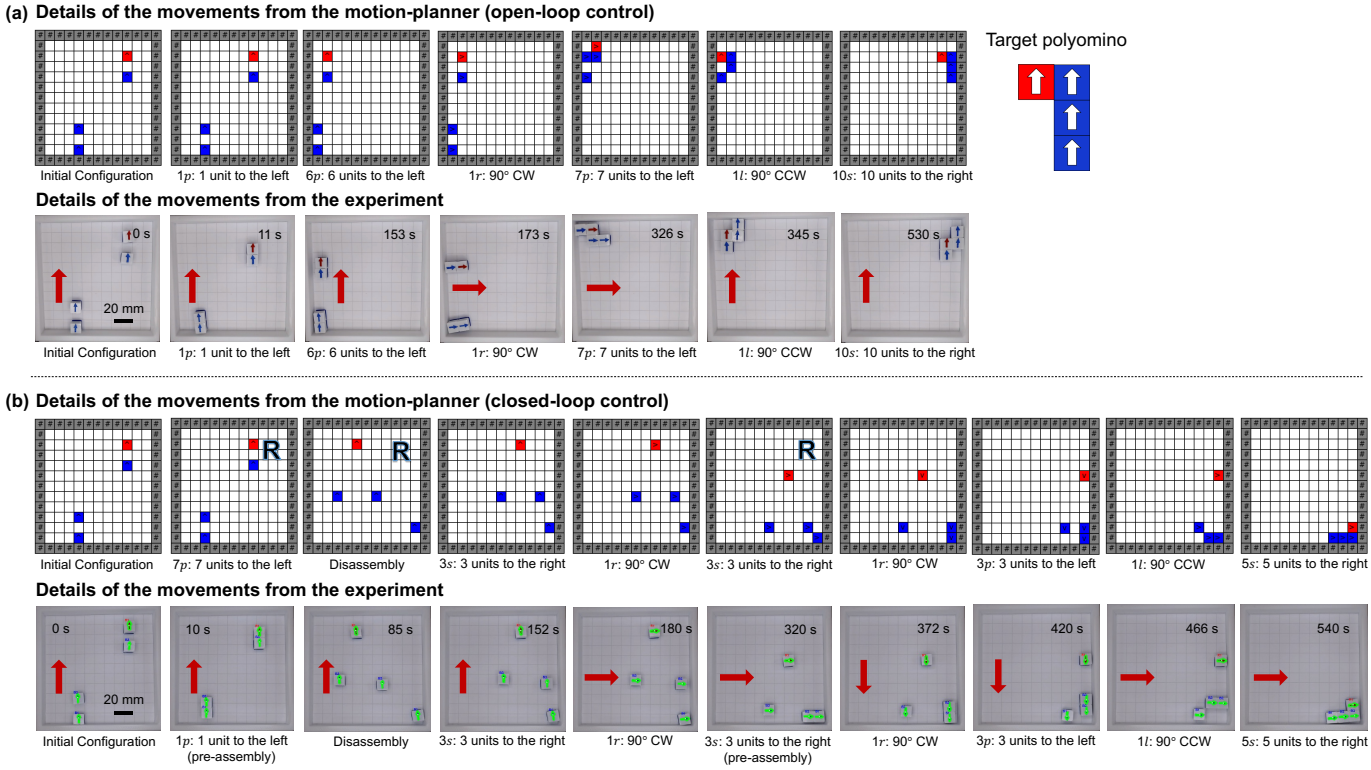

Fig. 7. Comparison of the open-loop and closed-loop controlled self-assembly to form the target L-shape polyomino using cubes with 10 mm edges. **(a)** Details of movements from the motion planner and video snapshots showing a failure during open-loop implementation. **(b)** Details of movements from the motion planner and snapshots from the motion tracker showing closed-loop implementation. **R** indicates the motion planner re-plans the path to follow based on the current configuration from the hardware. Red arrows point in the direction of the applied magnetic field. See video 2 for the demonstration.

V. Experimental Results

Several experiments were conducted to test the functionality of the closed-loop control pipeline with the new motion planner. Separate experiments were conducted for the cubes with 10 mm edge lengths and the smaller cubes with 2.8 mm edge lengths. For 10 mm cubes, the magnitude of the magnetic flux density was 15 mT for actuating individual cubes, but it was increased to 18 mT for actuating sub-assemblies and 23 mT for disassembly operations. For 2.8 mm cubes, the magnitude of the magnetic flux density was 18 mT for actuating individual cubes, but it was increased to 21 mT for actuating sub-assemblies and disassembly operations.

A. Self-assembly to form target colored polyominoes

Figure 4 shows three examples of using cubes with 10 mm edge lengths, starting with sub-assemblies to self-assemble a single structure using vision-based feedback. Because no pre-assembly occurred during the movements, cubes followed the original path generated by the motion planner and formed the target polyominoes as expected. To compare this method with open-loop control [18], we conducted five experiment trials for each target shape shown in Fig. 4 using open-loop control. The configurations in Figs. 4(a) and (b) failed to form the target shapes in all five trials, resulting in a 0 % success rate, whereas the configuration in Fig. 4(c) had a 100 % success rate. Open-loop works best when using a small number of cubes or when using a small number of sub-assemblies with the same shape. As we increase the number of cubes and/or the number of distinct shapes, the assembly process becomes more complex, leading to failures under open-loop control.

However, pre-assembly occurs more often for other configurations, especially when beginning with individual cubes, leading to undesired structures. Figures 6(b) and 7(b) show experimental results with closed-loop control of MMCs (10 mm edge lengths) using re-planning to form a target polyomino that could not be constructed with open-loop control (Figs. 6(a) and 7(a)). The target polyomino is I-shaped in Fig. 6, with all cubes connected in serial and two red cubes between the two blue cubes. Starting from the initial configuration shown in Fig. 6(a) at 0 s, the original path calculated by the motion planner commands cubes to: move right 4 units by pivot walking, rotate 90° CW, move right 7 units, rotate 90° CW, move right 8 units, rotate 90° CCW, and finally, move right 1 unit. However, the blue and red cubes prematurely self-assembled during the move right 4 units command, as they were brought in close proximity during pivot walking (Fig. 6(a) at 92 s). Because the bottom blue and red cubes were pre-assembled in parallel, these two subassemblies (serial- and parallel-connected assembly) cannot form the target polyomino, with all cubes having a serial connection. In the end, an L-shape polyomino (instead of the target I-shape) was formed by following the original path calculated by the motion planner in open-loop (Fig. 6(a) at 497 s). This was fixed using closed-loop control with re-planning as shown in Fig. 6(b). Starting with the same initial configuration, cubes were pre-

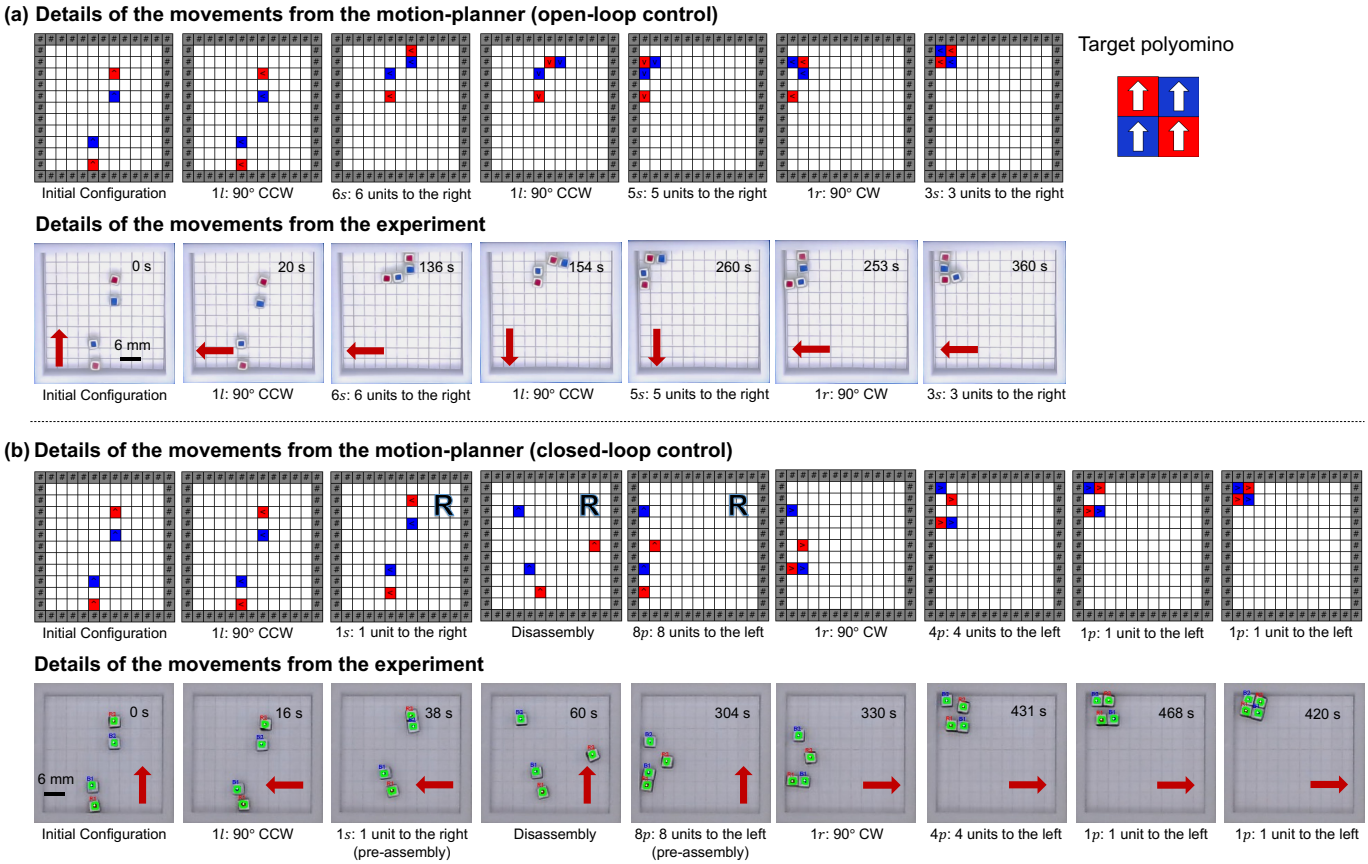

Fig. 8. Comparison of the open-loop and closed-loop controlled self-assembly to form the target square-shape polyomino using cubes with 2.8 mm edges. **(a)** Details of movements from the motion planner and video snapshots showing a failure during open-loop implementation. **(b)** Details of movements from the motion planner and snapshots from the motion tracker showing closed-loop implementation. **R** indicates the motion planner re-plans the path to follow based on the current configuration from the hardware. Red arrows point in the direction of the applied magnetic field. See video 2 for the demonstration.

assembled into two subassemblies at 50 s. Then the motion planner checked if the target polyomino was still reachable from the current configuration. However, the motion planner could not find a path to form the target polyomino from the configuration shown at 50 s. Therefore, the cubes were disassembled, resulting in a new configuration at 75 s. The motion planner could recalculate a path from this configuration, as shown in Fig. 6(b) at 127 s. **R** indicates when the motion planner re-plans a path based on the current configuration from the hardware. At 127 s, this includes a disassembly process and recalculation of the path. Figure 6(b) at 180 s shows that cubes prematurely self-assembled again during pivot walking; however, the motion planner still could generate a path to form the target I-shape polyomino from the current configuration, so no disassembly process was applied. Cubes followed the new path calculated from the motion planner and finally formed the target polyomino at 470 s. However, the success rate is relatively low (40%, with two successes out of five trials).

Figure 7 shows another example comparing open-loop control with closed-loop control using re-planning with cubes having 10 mm edges. The target polyomino is an L-shape polyomino with all blue cubes connected in serial and one red cube connected on the top left of the serial connected blue cubes. The initial configuration is shown in Fig. 7(a) at 0 s. The original path generated from the motion planner is "7p, 1r, 7p, 1l, 10s". However, when cubes followed the path to move left 1 unit, the top red and blue cubes were pre-assembled in serial at 11 s. Therefore, the target L-shape polyomino was not reachable by following the initial path in open-loop control, and finally, a Z-shape polyomino was formed (Fig. 7 at 530 s). Figure 7(b) shows the experimental results using closed-loop control to form the target L-shape polyomino from the same initial configuration. Because the target polyomino cannot be formed from the configuration shown in Fig. 7(b) at 10 s, the motion planner generated a disassembly step and re-planned the path to follow from the configuration after disassembly at 85 s. During the movement, cubes prematurely self-assembled again at 320 s as shown in Fig. 7(b), and the motion planner re-planned the path to follow based on the current configuration in the hardware and finally formed the target L-shape polyomino at 540 s.

Figure 8 compares open-loop control and closed-loop control with re-planning using cubes with 2.8 mm edges to form a square-shape polyomino. When cubes followed the path to move right after rotation, the red and blue cubes were pre-assembled at 136 s (a serial-connected assembly and a parallel-connected assembly) in Fig. 8(a). Therefore, following the original path in open-loop control, the target square-shaped polyomino was unreachable. Finally, an L-shape polyomino was formed (Fig. 8 at 360 s). Figure 8(b) shows the exper-

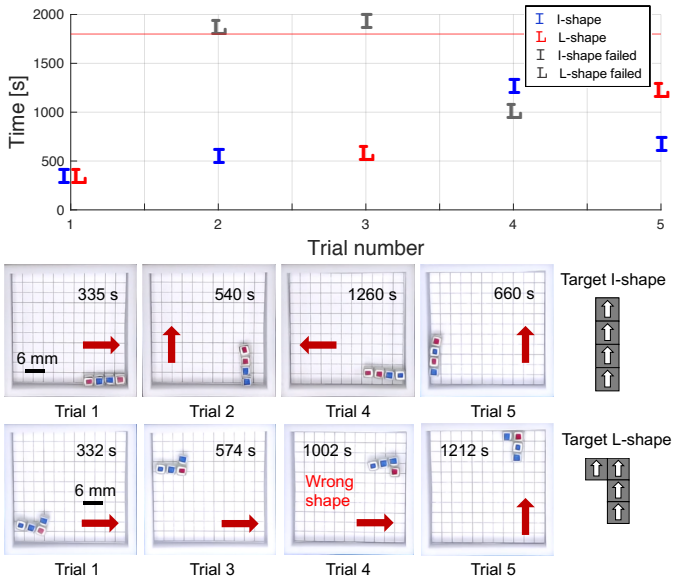

Fig. 9. Plots showing experimental results of forming the target I-shape in Fig. 6 and L-shape in Fig. 7 using cubes with 2.8 mm edges in five experimental trials. Any trial that did not form the target shape within 30 minutes (red horizontal line) or formed a wrong shape was recorded as a failure event (colored in gray). The red arrows indicate the direction of the applied magnetic field. See video 3 for these demonstrations.

imental result of forming the square-shape polyomino using closed-loop control with re-planning.

B. Self-assembly to form target shapes (arbitrary coloring)

To further improve the success rate, we use our method that only considers the shape, not the coloring of the cubes. Figure 9 shows the experimental results of forming the target I-shape (with all cubes assembled in serial) in Fig. 6 and the L-shape (with three cubes assembled in serial and one assembled on the top left) in Fig. 7 using cubes with 2.8 mm edge lengths. Starting from the same initial configuration shown in Fig. 6 and Fig. 7, we ran five experimental trials for each target shape. Any trial that did not form the target shape within 30 min was recorded as a failure (trial 3 for the I-shape and trial 2 for the L-shape). Trial 4 for the L-shape successfully formed an L-shape; however, the red cube assembled to the wrong side, which also counts as a failure. Therefore, the success rate of forming the target I-shape was 80%, and the success rate of forming the target L-shape was 60%. Both are better than the 40% success rate of forming an I-shape polyomino with a specified coloring.

VI. Conclusion

This paper presents a method for closed-loop control of magnetic modular cubes using computer vision-based feedback with re-planning to perform 2D self-assembly tasks. We tested the closed-loop control pipeline using cubes with 10 mm and cubes with 2.8 mm edge lengths. The experimental results demonstrate that using closed-loop control improves the success rate of forming user-specified polyominoes. Closed-loop control can also generate polyominoes that could not be constructed using open-loop control by disassembly and re-planning. We also proposed a method to improve the success rate by only considering the target shape. Future work will focus on 3D self-assembly using closed-loop control, building a high-fidelity physical simulation, and placing markers on the cubes to optimize the rotation command.

References

[1] I. Chen, M. Yim *et al.*, "Modular robots," in *Springer Handbook of Robotics*. Springer, 2016, pp. 531–542.
[2] U. K. Cheang, F. Meshkati, H. Kim, K. Lee, H. C. Fu, and M. J. Kim, "Versatile microrobotics using simple modular subunits," *Sci. Rep.*, vol. 6, 30472, 2016.
[3] H. Xie, M. Sun, X. Fan, Z. Lin, W. Chen, L. Wang, L. Dong, and Q. He, "Reconfigurable magnetic microrobot swarm: Multimode transformation, locomotion, and manipulation," *Sci. Rob.*, vol. 4, no. 28, p. eaav8006, 2019.
[4] J. Liu, X. Zhang, and G. Hao, "Survey on research and development of reconfigurable modular robots," *Adv. Mech. Eng.*, vol. 8, no. 8, 2016.
[5] S. Chennareddy, A. Agrawal, and A. Karuppiah, "Modular self-reconfigurable robotic systems: a survey on hardware architectures," *J. Rob.*, 2017.
[6] R. Fitch and Z. Butler, "Million module march: Scalable locomotion for large self-reconfiguring robots," *Int. J. Rob. Res.*, vol. 27, no. 3-4, pp. 331–343, 2008.
[7] G. Jing, T. Tosun, M. Yim, and H. Kress-Gazit, "An end-to-end system for accomplishing tasks with modular robots: Perspectives for the ai community." in *IJCAI*, 2017, pp. 4879–4883.
[8] R. Moreno, F. Veenstra, D. Silvera, J. Franco, O. Gracia, E. Cordoba, J. Gomez, and A. Faina, "Automated reconfiguration of modular robots using robot manipulators," in *SSCI*. IEEE, 2018, pp. 884–891.
[9] J. J. Abbott, E. Diller, and A. J. Petruska, "Magnetic methods in robotics," *Annu. Rev. Control Rob. Auton. Syst.*, vol. 3, no. 1, pp. 57–90, 2020.
[10] W. Saab, P. Racioppo, and P. Ben-Tzvi, "A review of coupling mechanism designs for modular reconfigurable robots," *Robotica*, vol. 37, no. 2, pp. 378–403, 2019.
[11] E. Diller, C. Pawashe, S. Floyd, and M. Sitti, "Assembly and disassembly of magnetic mobile micro-robots towards deterministic 2-d reconfigurable micro-systems," *Int. J. Rob. Res.*, vol. 30, no. 14, pp. 1667–1680, 2011.
[12] H. Gu, Q. Boehler, D. Ahmed, and B. J. Nelson, "Magnetic quadrupole assemblies with arbitrary shapes and magnetizations," *Sci. Robot.*, vol. 4, no. 3, eaax8977, 2019.
[13] L. W. Rogowski, A. Bhattacharjee, X. Zhang, G. Kararsiz, H. C. Fu, and M. J. Kim, "Magnetically programmable cuboids for 2d locomotion and collaborative assembly," in *2020 IEEE/RSJ International Conference on Intelligent Robots and Systems (IROS)*. IEEE, 2020, pp. 3326–3332.
[14] N. Ebrahimi, C. Bi, D. J. Cappelleri, G. Ciuti, A. T. Conn, D. Faivre, N. Habibi, A. Hošovskỳ, V. Iacovacci, I. S. Khalil *et al.*, "Magnetic actuation methods in bio/soft robotics," *Adv. Funct. Mater.*, vol. 31, no. 11, p. 2005137, 2021.
[15] X. Kuang, S. Wu, Q. Ze, L. Yue, Y. Jin, S. M. Montgomery, F. Yang, H. J. Qi, and R. Zhao, "Magnetic dynamic polymers for modular assembling and reconfigurable morphing architectures," *Adv. Mater.*, vol. 33, no. 30, p. 2102113, 2021.
[16] G. Barequet and M. Shalah, "Improved upper bounds on the growth constants of polyominoes and polycubes," *Algorithmica*, vol. 84, no. 12, pp. 3559–3586, 2022.
[17] Y. Lu, A. Bhattacharjee, D. Biediger, M. Kim, and A. T. Becker, "Enumeration of polyominoes & polycubes composed of magnetic cubes," in *2021 IEEE/RSJ International Conference on Intelligent Robots and Systems (IROS)*. IEEE, 2021, pp. 6977–6982.
[18] A. Bhattacharjee, Y. Lu, A. T. Becker, and M. Kim, "Magnetically controlled modular cubes with reconfigurable self-assembly and disassembly," *IEEE Trans. Rob.*, vol. 38, no. 3, pp. 1793–1805, 2022.
[19] B. Styler and R. Simmons, "Plan-time multi-model switching for motion planning," in *Proceedings of the International Conference on Automated Planning and Scheduling*, vol. 27, 2017, pp. 558–566.
[20] J. Tordesillas, B. T. Lopez, J. Carter, J. Ware, and J. P. How, "Real-time planning with multi-fidelity models for agile flights in unknown environments," in *ICRA*. IEEE, 2019, pp. 725–731.
[21] J. J. Abbott, "Parametric design of tri-axial nested helmholtz coils," *Rev. Sci. Instrum.*, vol. 86, no. 5, p. 054701, 2015.